Virology 535 (2019) 144–153

Contents lists available at ScienceDirect

Virology

journal homepage: www.elsevier.com/locate/virology

The cysteine-rich region of a baculovirus VP91 protein contributes to the morphogenesis of occlusion bodies

Fengqiao Zhou[a,b], Wenhua Kuang[a,c], Xi Wang[a,b], Dianhai Hou[a], Huachao Huang[a], Xiulian Sun[a], Fei Deng[a], Hualin Wang[a], Monqiue M. van Oers[d], Manli Wang[a,**], Zhihong Hu[a,*]

[a] State Key Laboratory of Virology and Joint-lab of Invertebrate Virology, Wuhan Institute of Virology, Chinese Academy of Sciences, Wuhan, 430071, PR China
[b] University of Chinese Academy of Sciences, Beijing, 10049, PR China
[c] Tongji Medical College, Huazhong University of Science and Technology, Wuhan 430030, PR China
[d] Laboratory of Virology, Wageningen University and Research, 6708, PB Wageningen, the Netherlands

ARTICLE INFO

Keywords:
VP91
Oral infection
Per os infectivity factor (PIF)
PIF8
Occlusion body (OB)
Cysteine-rich region
Disulfide bond
P33
HA76
Polyhedra

ABSTRACT

The baculovirus core gene *vp91* has been reported to be essential for nucleocapsid assembly and oral infection. Here, we studied the function of *vp91* by analyzing its homologue, *ha76*, in Helicoverpa armigera nucleopolyhedrovirus (HearNPV). HA76 was expressed at the late stage of HearNPV infection; deletion of *ha76* showed that the gene is required for budded virus production. A series of recombinants with truncated *ha76* was constructed and analyzed *in vitro* and *in vivo*. The results showed that the region encoding the C-terminus of HA76 was essential for nucleocapsid assembly, whereas the N-terminal cysteine-rich region was responsible for oral infection. Electron microscope analyses further showed that the cysteine-rich region contributed to morphogenesis of occlusion bodies (OBs), with amino acids 136–223 of HA76 being critical for this function. The results revealed a novel function of VP91 and suggested that the impact on OB morphogenesis is partially related to oral infectivity.

1. Introduction

Baculoviruses constitute large DNA viruses isolated from insects of the orders Lepidoptera, Hymenoptera, and Diptera. The family *Baculoviridae* contains four genera including *Alphabaculovirus*, *Betabaculovirus*, *Gammabaculovirus*, and *Deltabaculovirus* (Harrison et al., 2018). The alphabaculoviruses can be further divided into Group I and Group II based on phylogenetic analysis. During a typical alphabaculovirus infection, two kinds of progeny viruses are produced: budded viruses (BVs) and occlusion-derived viruses (ODVs). BVs are responsible for cell-to-cell transmission, whereas ODVs embedded in occlusion bodies (OBs) are responsible for *per os* infection in the insect midgut. BVs and ODVs share the same nucleocapsids but differ in their envelope proteins, which are responsible for their distinct functions (Hou et al., 2013). To date, more than 80 baculovirus genomes have been sequenced, with genome size ranging from 80 to 180 kb with 80–160 open reading frames (ORFs). A total of 38 conserved core genes are present in all sequenced baculoviral genomes (Rohrmann, 2013; Liu et al., 2016). These core genes serve essential roles in different processes of virus infection such as transcription, DNA replication, nucleocapsid assembly, BV/ODV production, and *per os* infection.

VP91 is encoded by one of these core genes and appears to have multiple functions. VP91 was originally characterized in Orgyia pseudotsugata nucleopolyhedrovirus (OpMNPV) as a late gene product with a size of 91 kDa, which is localized in the nucleocapsids of both BVs and ODVs (Russell and Rohrmann, 1997). Its homologue, *p95*, in Bombyx mori nucleopolyhedrovirus (BmNPV) encodes a protein containing putative DNA-binding and transcriptional activation regions that was able to stimulate gene expression driven by its own promoter or the host *actin* promoter (Lu et al., 1998). Deletion of *p95* in BmNPV showed that the gene is essential for BV production and nucleocapsid assembly (Xiang et al., 2013). Recent studies showed that the VP91 of Autographa californica nucleopolyhedrovirus (AcMNPV) is involved in both *per os* infection and nucleocapsid assembly, with these two functions seemingly regulated by different domains (Huang et al., 2017; Zhu et al., 2013; Javed et al., 2017). VP91 of AcMNPV contains a functional inner-nuclear membrane sorting motif (INM-SM) at its N-terminus (aa 1–38) (Zhu et al., 2013), followed by a cysteine-rich region (aa 135–402) and a short proline-rich domain (aa 671–698) at the C-terminus (Javed et al., 2017). Although initially it was suggested that a

* Corresponding author. Wuhan Institute of Virology, Chinese Academy of Sciences, Xiaohongshan No. 44, Wuhan, 430071, PR China.
** Corresponding author. Wuhan Institute of Virology, Chinese Academy of Sciences, Xiaohongshan No. 44, Wuhan, 430071, PR China.
E-mail addresses: wangml@wh.iov.cn (M. Wang), huzh@wh.iov.cn (Z. Hu).

https://doi.org/10.1016/j.virol.2019.06.016
Received 19 June 2019; Accepted 26 June 2019
Available online 03 July 2019
0042-6822/

C2H2 zinc finger (ZF) domain and a type II chitin binding domain (CBD) were contained within the cysteine-rich region (Zhu et al., 2013), further analysis indicated that the region might contain three C2H2 ZFs but no CBD (Javed et al., 2017). As the deletion of the cysteine rich region led to the total loss of oral infectivity, VP91 is therefore recognized as a *per os* infectivity factor (PIF8) (Javed et al., 2017). In addition, a 200 bp *cis*-acting element (nt 1651–1850) of *vp91* was found to be required for nucleocapsid assembly and termed the nucleocapsid assembly element (NAE). The NAE in AcMNPV contains eight conserved A/T-rich regions and functions in nucleocapsid assembly as a non-protein product (Huang et al., 2017).

As the current knowledge of VP91 function derives largely from AcMNPV and BmNPV, which are closely related group I alphabaculoviruses, it remains unclear whether the VP91 proteins of other baculoviruses have similar roles. In this study, we examined the structure and function of *ha76,* the gene encoding the VP91 homologue in Helicoverpa armigera nucleopolyhedrovirus (HearNPV), a group II alphabaculovirus (Chen et al., 2001). The amino acid identity between HA76 and the VP91 of AcMNPV is 46.3%. HearNPV has been widely used as a biological insecticide for controlling the cotton boll worm in China (Sun, 2015). We first characterized HA76 during HearNPV infection via transcription, expression, and cellular localization analyses. Subsequently, we generated a series of recombinant HearNPVs containing deleted, repaired, or truncated *ha76* based on bioinformatics analysis, and evaluated their impact on viral infection both *in vitro* and *in vivo*.

2. Materials and methods

2.1. Cells and viruses

The HzAM1 cell line, derived from *Heliothis zea* (Mcintosh and Ignoffo, 1983), was propagated in Grace's medium supplemented with 10% fetal bovine serum (Gibco-BRL, Gaithersburg, MD, USA) at 27 °C. The HearNPV G4 strain (Chen et al., 2001) was used in this study as the wild-type virus (WT). The HearNPV bacmid HaBacHZ8 (Wang et al., 2003) and the recombinant viruses HaBac-*egfp* and HaBac-*egfp-ph* were previously constructed in our laboratory (Song et al., 2008).

2.2. Antibodies

The region encoding aa 211–816 of HA76 was amplified from WT HearNPV using primers *ha76*exp-F and *ha76*exp-R (Table S1). The amplicons were cloned into the pET32a expression vector (Novagen, Madison, WI, USA) to generate pET32a-*ha76* and used for protein expression in *Escherichia coli* BL21 cells. The expressed protein was purified and used to immunize rabbits to generate a polyclonal anti-HA76 antibody. The antibodies against the major capsid protein VP39, BV Fusion (F) protein, and ODV-E66 of HearNPV were previously constructed in our laboratory (Deng et al., 2007; Long et al., 2006).

2.3. Temporal transcription and expression analyses of ha76

Monolayers of 1×10^6 HzAM1 cells were infected with HaBac-*egfp-ph* at a multiplicity of infection (MOI) of 5 ($TCID_{50}$/cell) and harvested at 0, 3, 6, 12, 24, 36, 48, and 72 h post infection (p.i.). For reverse transcription-polymerase chain reaction (RT-PCR), total RNA was extracted using TRIzol reagent (Invitrogen, Carlsbad, CA, USA) according to manufacturer protocol. RNA from each sample was treated with DNase I (Thermo) and tested by PCR to exclude DNA contamination.First strand cDNA was synthesized with the oligo (dT) primer using M-MLV reverse transcriptase (Promega, Madison, WI, USA). Specific primers *ha76*-SP-F and *ha76*-SP-R (Table S1) were used to amplify *ha76* transcripts.

Total proteins from cells collected at different time points post infection were loaded onto 12% sodium dodecyl sulfate-polyacrylamide gels for electrophoresis (SDS-PAGE) and Western blot analysis was performed using the anti-HA76 antibody (1:3000 dilution) as the primary antibody and horseradish peroxidase-labeled goat anti-rabbit antibody (1:5000 dilution; Merck-Sigma, St. Louis, MO, USA) as the secondary antibody. Western blot signal was visualized using the SuperSignal West Pico chemiluminescent substrate (Pierce, Rockford, IL, USA).

2.4. Subcellular localization of HA76 in HearNPV infected cells

The subcellular localization of HA76 during virus infection was analyzed by immunofluorescence assay. HzAM1 cells (1×10^6) on glass coverslips in 35 mm diameter culture dishes were infected with HaBac-*egfp-ph* at an MOI of 5. At 0, 12, 24, 48, and 72 h p.i., the cells were fixed with 4% (w/v) paraformaldehyde and permeabilized with 0.1% (v/v) Triton X-100. The cells were incubated with the anti-HA76 antibody (1:3000 dilution) overnight at 4 °C and subsequently incubated with the secondary antibody of goat anti-rabbit IgG H&L Alexa Fluor® 647 (Abcam, Cambridge, UK) for 1 h at room temperature. Hoechst 33258 (Beyotime, Shanghai, China) was used to stain the nuclei and the samples were analyzed by fluorescence microscopy (DeltaVision OMX Blaze™, GE Healthcare, Chicago, IL, USA).

2.5. Localization analysis of HA76 on BV and ODV

The BVs of WT HearNPV were harvested and purified from the supernatants of infected HzAM1 cells at 5 days p.i.(Braunagel and Summers, 1994). The OBs of WT HearNPV were purified from diseased larvae by differential centrifugation (Peng et al., 2011). To purify ODVs, OBs were incubated with DAS buffer (0.1 M Na_2CO_3, 0.5 M NaCl, 0.01 M ethylenediaminetetraacetic acid (EDTA), pH 10.9) at room temperature for 5 min, neutralized with 1/10 volume of neutralization buffer (0.5 M Tris–HCl, pH 7.5) for 2 min at room temperature, and then centrifuged at $800 \times g$ to remove cell debris. The supernatants were further centrifuged at $18{,}000 \times g$ (4 °C) for 30 min to collect ODVs. Then, the nucleocapsid and envelope fractions of BVs and ODVs were isolated according to a previously published procedure (Braunagel and Summers, 1994). Following purification, all samples were subjected to 12% SDS-PAGE and Western blot analyses were performed by using anti-HA76, as well as anti-VP39, anti-ODV-E66, and anti-F (1:3000 dilution) antibodies as the primary antibody to verify the expected fractions.

To detect the localization of HA76 in the recombinant viruses, the OBs of the recombinant viruses were pretreated at 85 °C for 30 min to inactivate the endogenous proteinase and the ODVs were purified as described above and subjected to Western blot analysis.

2.6. Bioinformatics analyses

HA76 was searched against the non-redundant protein sequences at the National Center for Biotechnology Information database using the position-specific iterated (PSI) BLAST algorithm to find all known homologues. The conserved domains of HA76 were predicted using PredictProtein (https://www.predictprotein.org/). Multiple sequence alignment was constructed using ClustalW with default parameters and manually edited with GeneDoc.

2.7. Construction of ha76-deleted, repaired, and truncated HearNPV bacmids

The *ha76* null bacmid was constructed using homologous recombination as described previously (Huang et al., 2012). Briefly, upstream and downstream fragments of *ha76* (approximately 500 bp each) were amplified using HaBacHZ8 as the template with the primers *ha*76UP-F/*ha*76UP-R and *ha*76DN-F/*ha*76DN-R, respectively (Table S1). The upstream- and downstream homologous arms were digested,

gel purified, and then cloned into pKS-*egfp-Cm*^{r} (provided by Dr. Just M. Vlak, Wageningen University and Research, The Netherlands). The linear fragment containing *egfp*, the chloramphenicol resistance gene *Cm*^{r}, and the *ha76* flanking sequences was PCR amplified with *ha76*UP-F and *ha76*DN-R and electroporated into *E. coli* BW25113 harboring HaBacHZ8 DNA and pKD46 (Wang et al., 2003). Positive clones were selected by chloramphenicol resistance and confirmed by PCR and sequencing. The correct bacmid was designated bHaBac*76KO*.

To re-introduce the *polyhedrin* gene (*ph*) and *ha76* into bHaBac*76KO*, the entire *ha76* coding sequence (aa 1–816) was amplified from the genome of HaBac-*egfp-ph* with *ha76Repair*-F and *ha76Repair*-R (Table S1) and cloned into the pFB-DUAL-*ph* transfer vector (Song et al., 2008) under the control of the *p10* gene promoter to generate pFB-*76*R-*ph*. Then, pFB-DUAL-*ph* and pFB-*76*R-*ph* were used individually to transform DH10B cells containing bHaBac*76KO* and pKD46. Positive clones were selected by gentamicin and kanamycin resistance with blue/white screening and further confirmed by PCR using M13F and M13R (Bac-to-Bac manual, Invitrogen). The resulting bacmids were designated as bHaBacΔ*76* and bHaBacΔ*76*-$R_{1–816}$, respectively. To investigate the function of HA76, a series bacmids with truncated versions of *ha76* were generated. Based on the results of bioinformatics analysis, the cysteine-rich region was further divided into three domains including CR1 (aa 136–223), CR2 (aa 223–282), and CR3 (aa 304–405). Truncated *ha76* genes with deletion of aa 406–816, 136–405 (CR1-3), 136223 (CR1), 223–283 (CR2), or 304–405 (CR3) were PCR amplified by using the corresponding primers listed in Table S1. Recombinant bacmids containing the truncated *ha76* and a restored *ph* were generated using similar methods as described above and designated as bHaBacΔ*76*-$R_{Δ406–816}$, bHaBacΔ*76*-$R_{ΔCR1–3}$, bHaBacΔ*76*-$R_{ΔCR1}$, bHaBacΔ*76*-$R_{ΔCR2}$, sand bHaBacΔ*76*-$R_{ΔCR3}$, respectively.

2.8. Transfection-infection assays

HzAM1 cells (6×10^5) were seeded into 35 mm cell culture dishes and allowed to attach overnight. Then, 1 μg DNA of each recombinant bacmid was used individually to transfect HzAM1 cells following the Bac-to-Bac manual (Invitrogen). At 120 h post transfection (p.t.), the samples were centrifuged to remove cell debris and the supernatants were used to infect a new batch of HzAM1 cells. Fluorescence microscopy images were recorded at 96 h p.t. or p.i. to detect virus replication. The BVs titers were analyzed in triplicate by end-point dilution assays.

2.9. One step growth curve analysis of the recombinant viruses

HzAM1 cells (1×10^6) were infected with an MOI of 5 of the recombinant viruses HaBacΔ76-$R_{1–816}$, HaBacΔ*76*-$R_{ΔCR1–3}$, HaBacΔ*76*-$R_{ΔCR1}$, HaBacΔ*76*-$R_{ΔCR2}$, or HaBacΔ*76*-$R_{ΔCR3}$ or control virus HaBac-*egfp-ph*. The supernatants were collected at 0, 24, 48, 72, and 96 h p.i., and BV titers were analyzed in triplicate using end-point dilution assays.

2.10. Electron microscopy

HzAM1 cells (5×10^5) were transfected with 5 μg DNA of bHaBacΔ*76* or bHaBacΔ*76*-$R_{406–816}$, or infected with recombinant viruses of HaBac-*egfp-ph*, HaBacΔ*76*-$R_{1–816}$, HaBacΔ*76*-$R_{ΔCR1–3}$, HaBacΔ*76*-$R_{ΔCR1}$, HaBacΔ*76*-$R_{ΔCR2}$, or HaBacΔ*76*-$R_{ΔCR3}$ at an MOI of 5. At 96 h p.t. or 96 h p.i., the cells were collected and prepared for electron microscopy as described previously (Kuang et al., 2016). Cells were observed by transmission electron microscopy (TEM) (FEI Tecnai G2 microscope at 200 kV; Eindhoven, The Netherlands). The number of ODVs from at least 20 cell-sections of each virus was determined, logarithm-transformed to fit normal distribution and analyzed by one-way ANOVA with SPSS 12.0 (SPSS, Inc. SPSS 12.0 Base User's Guide; Prentice Hall Chicago, IL, USA, 2003). If significant differences were found, Dunnett-t tests were used to compare ODVs numbers of the recombinant viruses with those of wild-type control.

To amplify the OBs of recombinant viruses, the BVs of HaBacΔ76-$R_{1–816}$, HaBacΔ*76*-$R_{ΔCR1–3}$, HaBacΔ*76*-$R_{ΔCR1}$, HaBacΔ*76*-$R_{ΔCR2}$, and HaBacΔ*76*-$R_{ΔCR3}$ were injected into the haemocoel of late fourth-instar *H. armigera* larvae. OBs were then extracted from diseased larvae by differential centrifugation (Peng et al., 2011). The purified OBs were observed by TEM and scanning electron microscopy (SEM) (HITACHII SU-8010; Tokyo, Japan) as described previously(Kuang et al., 2017).

To observe ODVs embedded within OBs, 10 μL of OB suspension (10^8 OBs mL^{-1}) was loaded onto a copper grid for 10 min; filter paper was used to remove the remaining solution from the grid. Then, 10 μL of 0.5 × dissolution buffer (0.1 M Na_2CO_3, 0.01 M EDTA, 0.15 M NaCl [pH 11]) was added to dissolve the OBs for 2 min; after removing the dissolution buffer, the grid was stained with 2% (wt/vol) phosphotungstic acid (pH 5.7) for 1 min. The grids were kept at room temperature overnight and observed with TEM. The data regarding the number of ODVs in each OB were collected and the comparison between the WT and recombinant viruses was analyzed by one-way ANOVA using SPSS 12.0 If significant differences were found, Dunnett t tests were used to compare the virus' ODVs number in OB with those of wild-type control.

2.11. Feeding assay and bioassay

The oral infectivity of WT HearNPV, HaBacΔ*76*-$R_{1–816}$, HaBacΔ*76*-$R_{ΔCR1–3}$, HaBacΔ*76*-$R_{ΔCR1}$, HaBacΔ*76*-$R_{ΔCR2}$, and HaBacΔ*76*-$R_{ΔCR3}$ was detected using the droplet method (Hughes et al., 1986) with early third-instar *H. armigera* larvae. For the feeding assay, 1×10^8 OBs mL^{-1} of each virus was used (Sun et al., 1997). For the bioassay, different concentrations of the OBs were used for different viruses. The WT HearNPV, HaBacΔ*76*-$R_{1–816}$, and HaBacΔ*76*-$R_{ΔCR3}$ were tested with the concentrations of 1×10^4, 3×10^4, 1×10^5, 3×10^5, and 1×10^6 OBs mL^{-1}, whereas HaBacΔ*76*-$R_{ΔCR2}$ was tested with the concentrations of 1×10^6, 1×10^7, 1×10^8, 3×10^8, and 1×10^9 OBs mL^{-1}. For all the oral infection experiments, the larvae were kept separately in 24 well plates and monitored daily until all the tested larvae had either pupated or died. At least 48 larvae were tested per treatment. Both the feeding assays and the bioassays were performed twice. The LD_{50} and 95% confidence interval (CI) of each virus were determined with a probit analysis using SPSS 12.0. The LD50 values of the recombinant viruses were compared to that of the WT HearNPV by a potency ratio method (Robertson et al., 2017).

3. Results

3.1. Ha76 is a late gene of HearNPV

To understand the function of *ha76*, we first characterized the gene transcription and protein expression by RT-PCR and Western blot analysis, respectively. HzAM1 cells were infected with HaBac-*egfp-ph* at 5 MOI and harvested at different times post infection. RT-PCR was performed with cDNA using *ha76* specific primers; RT-PCR products with expected size (approximately 730 bp) were detected from 12 to 72 h p.i. (Fig. 1A, upper panel). PCR of the same DNase-treated samples prior to reverse transcription did not show any positive band (data not shown). The transcription pattern of *ha76* is similar to that of AcMNPV *vp91* (Chen et al., 2013). The full-length HA76 protein contains 816 aa with a predicted molecular weight of 93.5 kDa. Western blot analysis detected a specific immune-reactive band of approximately 100 kDa from 24 to 72 h p.i., suggesting that HA76 likely undergoes some type of protein modification. In AcMNPV and OpMNPV, the monocular weights of the detected VP91s were also higher than predicted (Javed et al., 2017; Zhu et al., 2013; Russell and Rohrmann, 1997). An additional band of approximately 70 kDa was also detected from 36 to 72 h p.i., likely derived from cleavage or degradation of the protein, but

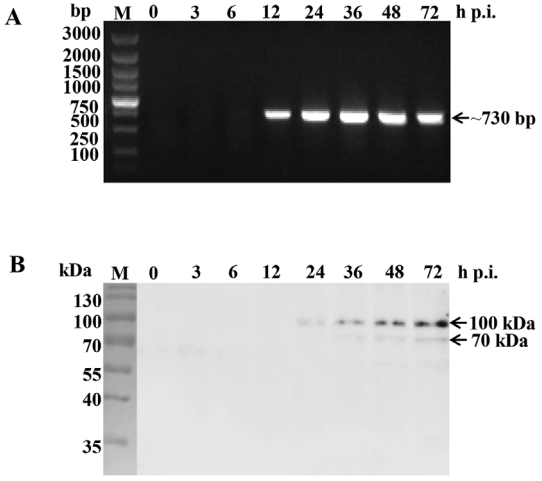

Fig. 1. Temporal analysis of HA76 transcription and expression in infected cells. HzAM1 cells infected with HaBac-*egfp-ph* at an MOI of 5 were harvested at the indicated time points. (A). Total RNA was extracted for detecting *ha76* transcripts by RT-PCR. (B). Total protein was subjected to Western blot analysis by using anti-HA76 as the primary antibody.

could also be the result of internal initiation of translation or even mRNA splicing (Fig. 1B). The transcription and expression data thus suggest that *ha76* is a late gene of HearNPV. Consistent with this, a late transcription initiation motif, TAAG, was found at 78 nucleotides (nt) upstream of the translational start codon.

3.2. HA76 localizes in the nuclear ring zone region at the late stage of virus infection

To explore the subcellular localization of HA76 during virus infection, HzAM1 cells were infected with HaBac-*egfp* at an MOI of 5, and cells collected at different time points were subjected to immunofluorescence assay. The results showed that the signal of HA76 was first detected at 24 h p.i., at which point it had already gathered around the ring zone of infected cell-nuclei, a locus for ODV assembly. This localization pattern remained largely unchanged at the later stages of infection (Fig. 2).

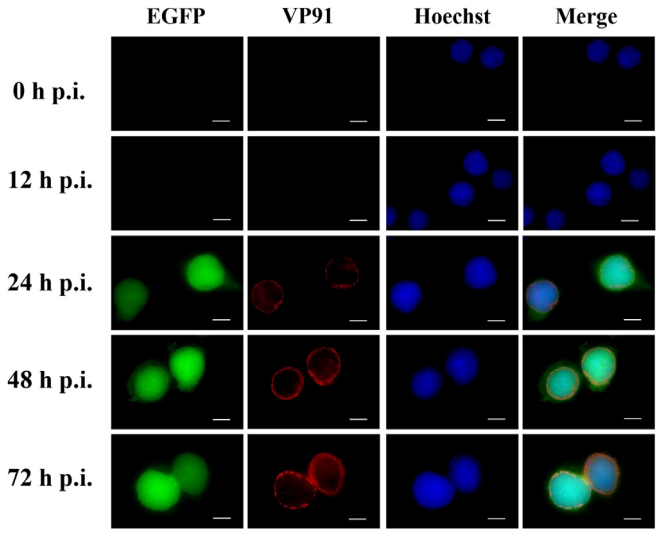

Fig. 2. Subcellular localization of HA76 in infected cells. HzAM1 cells were infected with HaBac-*egfp* at an MOI of 5 and harvested at the indicated time points. Cells were fixed and subjected to immunofluorescence analysisusing an anti-HA76 antibody (red). EGFP (green) indicated successful infection of the cells. The nuclei were stained with Hoechst 33258 dye (blue). Bars, 10 μm.

3.3. HA76 is a structural protein of ODV but not BV

To determine whether HA76 functions as a structural protein of HearNPV, Western blot analysis was conducted on the purified BV and ODV, along with their envelope and nucleocapsid fractions. The results showed that anti-HA76 detected as a specific band with a size of approximately 100 kDa localized in both the envelope and nucleocapsid fractions of ODV (Fig. 3A) but absent in BVs. (Fig. 3B). As controls, antibodies against the major capsid protein VP39, the BV envelope-specific F protein, and the ODV envelope specific ODV-E66 were used; these detected specific signals only in the expected fractions (Fig. 3). Thus, the results demonstrated that HA76 is an ODV-specific protein in HearNPV.

3.4. Bioinformatics analysis of HA76 and generation of a series of ha76 mutants

For further analysis of the structure and function of HA76, we conducted bioinformatics analyses. HA76 contains several conserved domains with VP91 of AcMNPV including a putative INM-SM (aa 6–26), a cysteine-rich region (aa 136–405), and a proline-rich region (PR, aa 643–667) (Fig. 4A, upper panel). VP91 is conserved across all baculoviruses and its homologues are also found in nudiviruses (Yang et al., 2014; Wang et al., 2007; Burand et al., 2012). Bioinformatics analyses suggested that the cysteine-rich region could be further broken down into three domains (CR1–3) based on conservation among the VP91 homologues. CR1 is conserved in all VP91 homologues; however, CR2 appears to be missing in betabaculoviruses, whereas CR3 is truncated in nudiviruses (Fig. 4A, lower panel). Moreover, although a previous study of AcMNPV VP91 identified three ZF motifs in these domains (Javed et al., 2017), our analysis indicated that among other baculoviruses, the ZF motif is only conserved in the CR1 domain, but not in CR2 and CR3 (Fig. S1).

Based on the bioinformatics data, a series of recombinant HearNPV bacmids containing different versions of HA76 were constructed and verified. These included the *ha76* deletion bacmid bHaBacΔ76, repaired bacmid bHaBacΔ*76-R*$_{1–816}$, and truncated bacmids bHaBacΔ*76-R*$_{406–816}$, HaBacΔ*76-R*$_{\Delta CR1–3}$, HaBacΔ*76-R*$_{\Delta CR1}$, HaBacΔ*76-R*$_{\Delta CR2}$ and HaBacΔ*76-R*$_{\Delta CR3}$ (Fig. 4B). All the recombinant bacmids contained *egfp* and *ph* for monitoring virus infection *in vitro* and *in vivo*.

3.5. Ha76 is essential for BV production

Following transfection of the recombinant bacmids into HzAM1 cells, fluorescent cells were observed at 24 h p.t. indicating successful transfections with all bacmids (data not shown). At 96 h p.t., spreading and infection of adjoining cells was observed in the majority of transfected cells except for those transfected by bHaBacΔ*76* or HaBacΔ*76-R*$_{\Delta 406–816}$ (Fig. 4C). Subsequent infection assays with the supernatant of transfected cells confirmed that HaBacΔ*76* and HaBacΔ*76-R*$_{\Delta 406–816}$ were unable to produce infectious progeny BVs (Fig. 4C).

To further investigate the effects of HA76 truncations on infectious BV production, one step growth curve analyses were conducted with recombinant viruses of HaBac-*egfp-ph*, HaBacΔ*76-R*$_{1–816}$, HaBacΔ*76-R*$_{\Delta CR1–3}$, HaBacΔ76-*R*$_{\Delta CR1}$, HaBacΔ*76-R*$_{\Delta CR2}$, and HaBacΔ*76-R*$_{\Delta CR3}$ at an MOI of 5. As shown in Fig. 4D, all recombinant viruses exhibited similar replication kinetics to that of the control virus HaBac-*egfp-ph*. As HaBacΔ*76-R*$_{\Delta 406–816}$ completely lost the ability for BV production whereas HaBacΔ*76-R*$_{\Delta CR1–3}$ provided BV titer at WT level, the data suggested that the region encoding aa 406–816 of HA76 is likely responsible for BV production.

3.6. Ha76 is essential for nucleocapsid assembly

To determine the effect of *ha76* deletion on virus morphogenesis, HzAM1 cells were transfected with bHaBacΔ*76* or bHaBacΔ*76-R*$_{\Delta 406–816}$

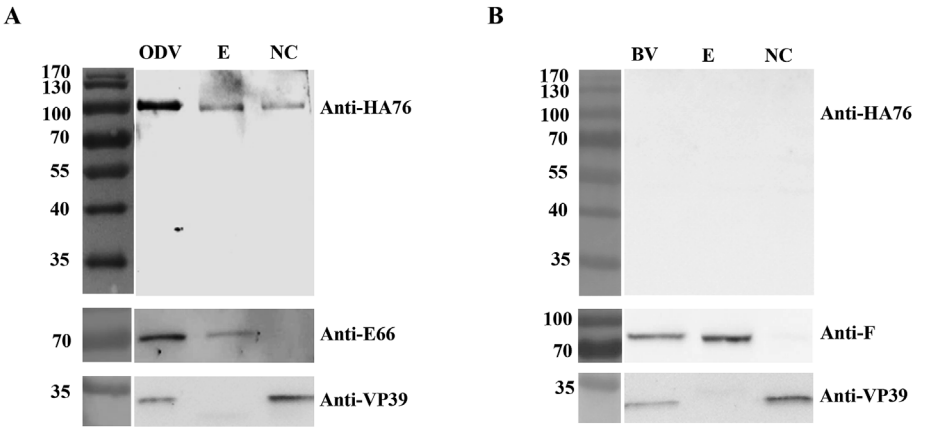

Fig. 3. Western blot analyses of HA76 in the envelope and nucleocapsid fractions of occlusion-derived viruses (ODVs) and budded viruses (BV). (A). Western blot analyses were performed with purified ODVs and the envelope or nucleocapsid fractions of the ODVs using an anti-HA76 antibody. (B). Detection of HA76 in the purified BVs and envelope/nucleocapsid fractions of the BVs. The quality of the fractionation was verified by using antisera against the nucleocapsid protein VP39, the ODV envelope-specific protein ODV-E66, and the BV envelope-specific protein F.

(both had failed to form BV), or infected with HaBacΔ*76*-$R_{1–816}$, HaBacΔ*76*-$R_{\Delta CR1–3}$, HaBacΔ*76*-$R_{\Delta CR1}$, HaBacΔ*76*-$R_{\Delta CR2}$, HaBacΔ*76*-$R_{\Delta CR3}$, or the control virus HaBac-*egfp-ph*, and examined by TEM. The result showed that similar to effects of the control virus HaBac-*egfp-ph* (data not shown), cells infected with HaBacΔ*76*-$R_{1–816}$ displayed typical phenomena of baculovirus infection including virogenic stroma interspersed with rod shaped electron-dense nucleocapsids (data not shown) and multiple matured enveloped nucleocapsids within the ring zone or embedded in the developing OBs (Fig. 5). However, in bHaBacΔ*76* or bHaBacΔ*76*-$R_{\Delta 406–816}$-transfected cells, no properly assembled nucleocapsids were detected within the nucleus, and empty OBs were observed (Fig. 5). The data suggested that *ha76*, specifically the region encoding aa 406–816 of HA76, is essential for nucleocapsid assembly. This is in agreement with the finding that the same region is essential for BV production. This region covers the NAE region (nt 1651–1850) identified in Ac83 (Huang et al., 2017). In the cells infected with other recombinant viruses, no obvious impact on nucleocapsid assembly was observed, but the OBs in the cells infected with HaBacΔ*76*-$R_{\Delta CR1-3}$ and

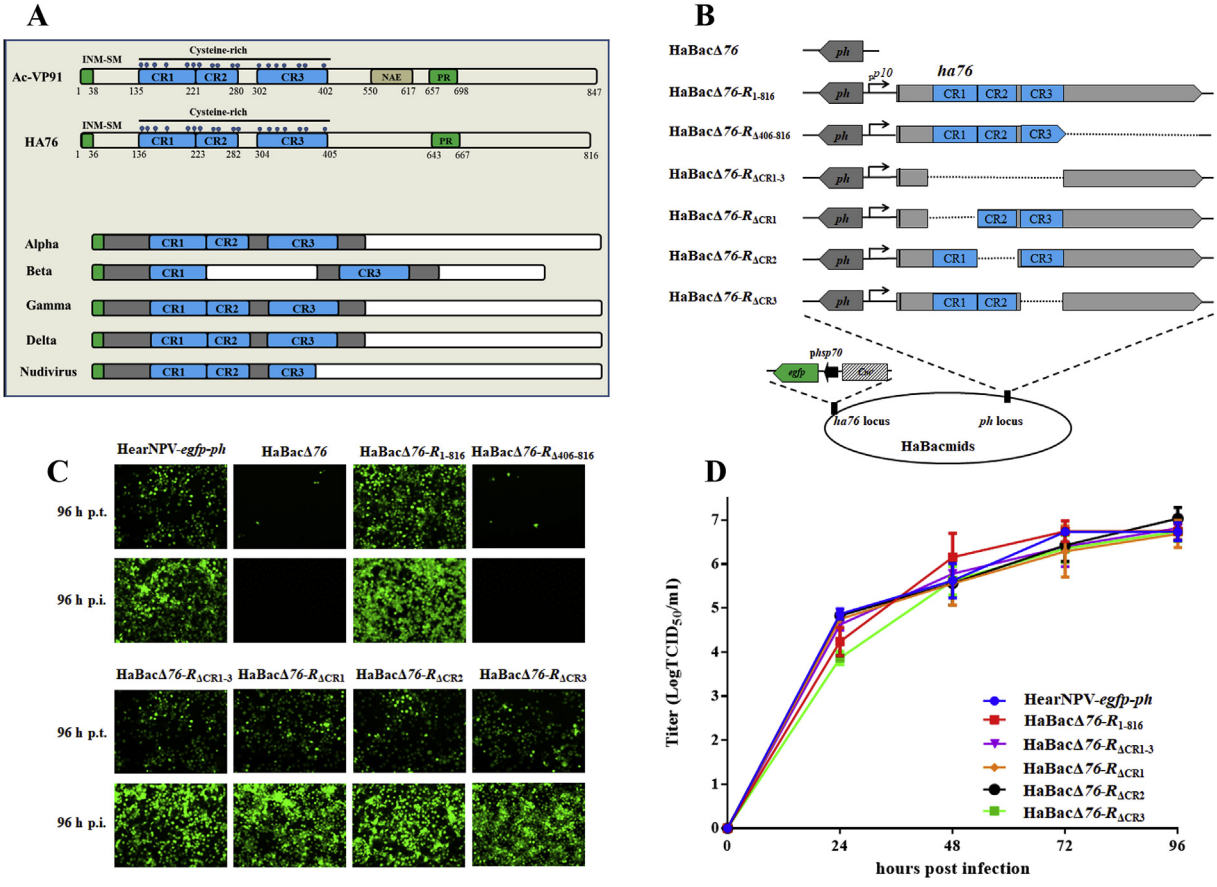

Fig. 4. Construction and identification of the recombinant viruses. (A). Bioinformatics analyses of HA76 and VP91 homologues. Upper panel: schematic diagrams showing conserved domains of HA76 and AcMNPV VP91. The cysteines are indicated by dots above the diagrams. INM-SM: inner nuclear membrane-sorting motif; CR: cysteine-rich region. NAE: nucleocapsid assembly element. PR: proline rich region. Lower panel: schematic diagrams showing representative VP91s of viruses in the different genera of the family *Baculoviridae* and in the *Nudiviridae*. Dark grey indicates relatively conserved regions between different viruses, whereas white represents regions of low homology. (B). Schematic diagrams of the recombinant viruses. (C). Transfection-infection assay of recombinant bacmids. Fluorescence microscopy to detect EGFP was performed at 96 h p.t. or 96 h p.i. (D). One-step growth curve of the recombinant viruses. Bars, standard deviations of the mean of three replicates.

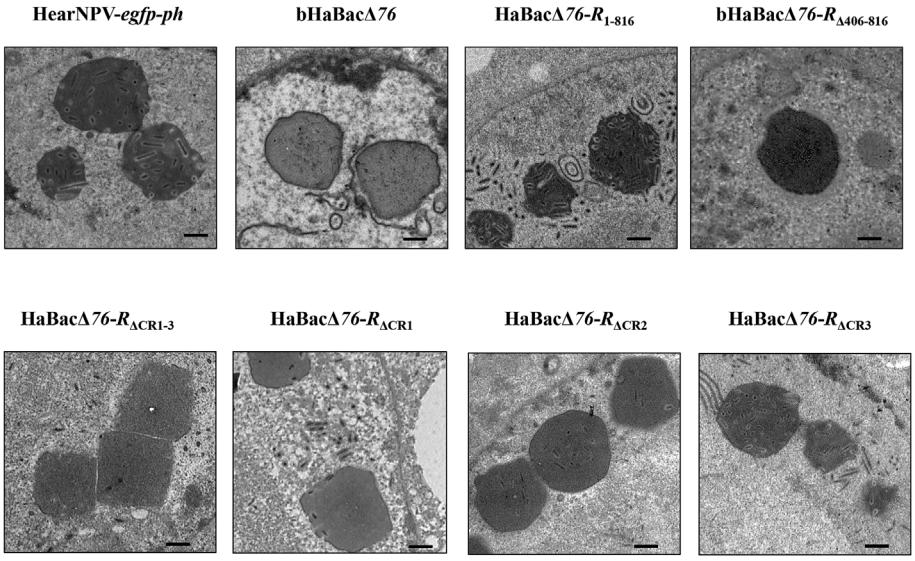

Fig. 5. Transmission electron microscopy (TEM) analysis of HzAM1 cells transfected/infected with different recombinants. HzAM1 cells were transfected with bHaBacΔ*76-ph* and bHaBacΔ*76-*$R_{\Delta 400–816}$, or infected with HearNPV-*egfp-ph*, HaBacΔ*76-*$R_{1–816}$, HaBacΔ*76-*$R_{\Delta CR1-3}$, HaBacΔ*76-*$R_{\Delta CR1}$, HaBacΔ*76-*$R_{\Delta CR2}$, or HaBacΔ*76-*$R_{\Delta CR3}$. The cells were harvested at 96 h p.t. or 96 h p.i. for TEM. Bars, 500 nm.

HaBacΔ*76-*$R_{\Delta CR1}$ appeared to contain less ODVs (Fig. 5) and this phenomenon was further investigated.

3.7. The cysteine-rich region of HA76 is critical for OB morphogenesis

To clarify whether the embedding of ODVs in OBs was affected by HA76, the purified OBs of HaBacΔ*76-*$R_{1–816}$, HaBacΔ*76-*$R_{\Delta CR1–3}$, HaBacΔ*76-*$R_{\Delta CR1}$, HaBacΔ*76-*$R_{\Delta CR2}$, and HaBacΔ76-$R_{\Delta CR3}$ were analyzed with EM. The results of SEM (Fig. 6A) showed that the OBs of the repaired virus HaBacΔ*76-*$R_{1–816}$ presented normal morphology with a smooth surface and polyhedral shape, whereas those of HaBacΔ*76-*$R_{\Delta CR1–3}$ and HaBacΔ*76-*$R_{\Delta CR1}$ appeared to be abnormal and pitted. In comparison, the OBs of HaBacΔ*76-*$R_{\Delta CR2}$ and HaBacΔ*76-*$R_{\Delta CR3}$ were largely normal but their surfaces were not as smooth as that of the repaired virus (Fig. 6A).

The TEM results showed that the OBs of HaBacΔ*76-*$R_{\Delta CR1–3}$ and HaBacΔ*76-*$R_{\Delta CR1}$ were fragile, and there appeared to be fewer ODVs embedded in the OBs of HaBacΔ*76-*$R_{\Delta CR1–3}$ (Fig. 6B). The OBs of HaBacΔ*76-*$R_{\Delta CR2}$ and HaBacΔ*76-*$R_{\Delta CR3}$ appeared largely normal and showed no notable difference with those of the repaired virus (Fig. 6B).

Negative staining of the dissolved OBs showed that there were obviously fewer embedded ODVs in the OBs of HaBacΔ*76-*$R_{\Delta CR1–3}$ and HaBacΔ*76-*$R_{\Delta CR1}$ (Fig. 6C). To quantify the HA76 effect on ODV embedding, the average ODV numbers in OBs were calculated using at least 60 OBs for each virus (Fig. 7A). The ODV numbers (means ± standard deviations) were 35.6 ± 1.4, 35.9 ± 1.8, 5.2 ± 0.6, 24 ± 2.1, 32 ± 1.1, and 34.9 ± 2.1 for WT, HaBacΔ*76-*$R_{1–816}$, HaBacΔ*76-*$R_{\Delta CR1–3}$, HaBacΔ*76-*$R_{\Delta CR1}$, HaBacΔ*76-*$R_{\Delta CR2}$, and HaBacΔ*76-*$R_{\Delta CR3}$, respectively. No significant differences ($p > 0.05$) were observed between WT and HaBacΔ*76-*$R_{1–816}$ ($p = 0.894$), HaBacΔ*76-*$R_{\Delta CR2}$ ($p = 0.082$), or HaBacΔ*76-*$R_{\Delta CR3}$ ($p = 0.796$). In contrast, ODV numbers in WT significantly differed ($p < 0.05$) from those of HaBacΔ*76-*$R_{\Delta CR1–3}$ ($p = 1.73 \times 10^{-37}$) or HaBacΔ*76-*$R_{\Delta CR1}$ ($p = 4.51 \times 10^{-5}$). To determine if the recombinant viruses have impact on production of ODV, the ODV numbers in the nucleus of the infected cells were calculated using at least 20 cell-sections for each virus. The ODV numbers (means ± standard deviations) were 269.75 ± 27.9, 210.2 ± 18.9, 205.7 ± 16.5, 229.3 ± 21.2,

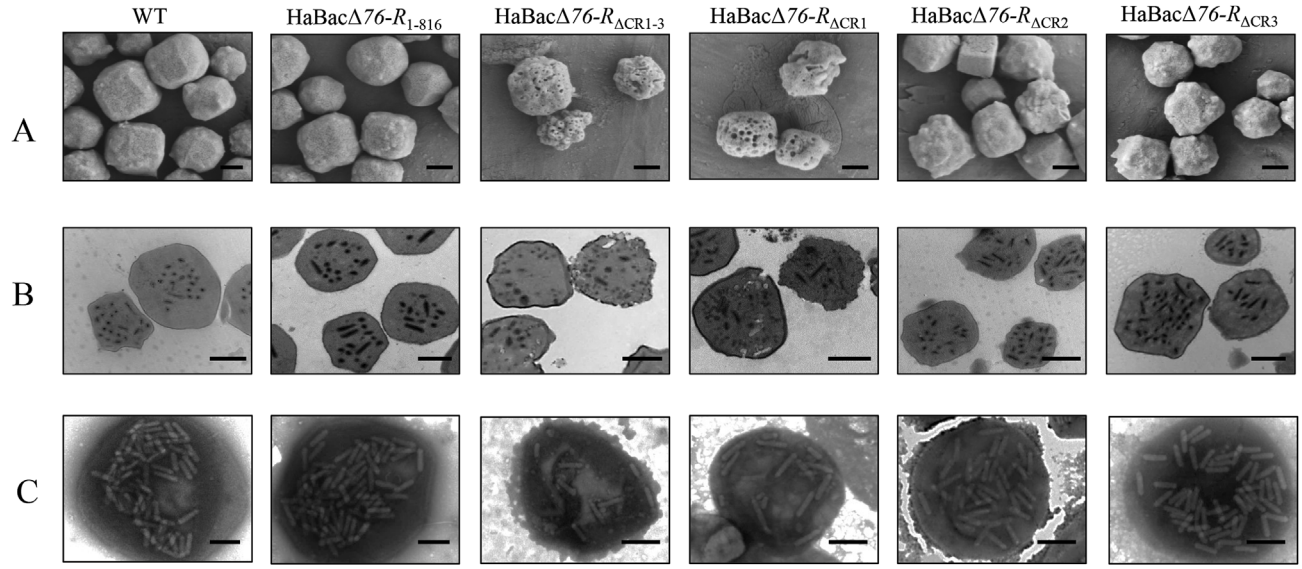

Fig. 6. Scanning electron microscopy (SEM), transmission electron microscopy (TEM), and negative staining analysis of WT and recombinant occlusion bodies (OBs). Purified OBs of WT, HaBacΔ*76-*$R_{1–816}$, HaBacΔ*76-*$R_{\Delta CR1–3}$, HaBacΔ*76-*$R_{\Delta CR1}$, HaBacΔ*76-R* $_{\Delta CR2}$, and HaBacΔ*76-*$R_{\Delta CR3}$ were subjected to SEM (A), TEM (B), and negative staining of dissolved OB (C) as described in Material and methods. Bars, 500 nm.

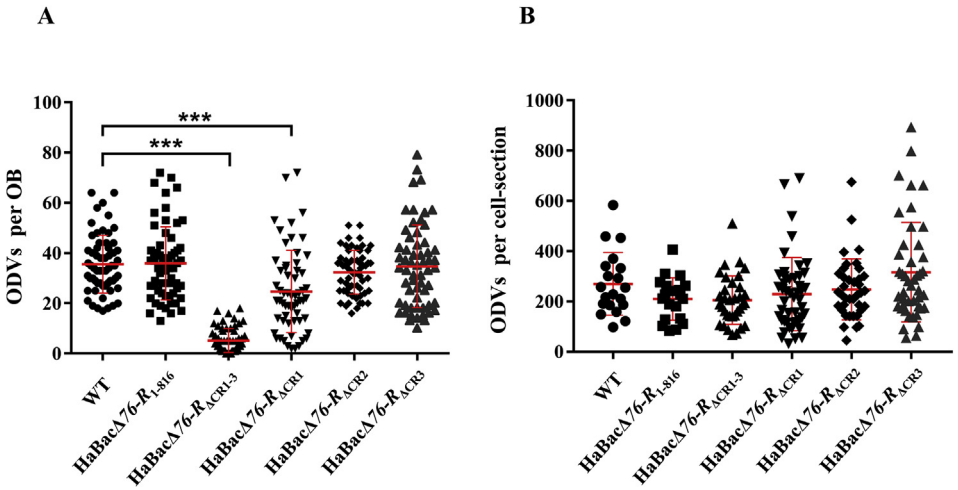

Fig. 7. Numbers of embedded or produced occlusion-derived viruses (ODVs) in WT and recombinant viruses. (A). Numbers of embedded ODVs in WT and recombinant occlusion bodies (OBs). The numbers of embedded ODVs in OBs were collected from individual OBs analyzed by negative staining (Fig. 6C). A total of 60 OBs for each virus were collected for analysis. Statistical analysis was determined using one-way analysis of variance (ANOVA) with SPSS software. Error bars indicate the average ODV numbers per OB (means ± standard deviations). (B). Numbers of produced ODVs in WT and recombinant viruses infected cells. At least 20 cell-sections of each virus were collected and statistical analyzed by one-way ANOVA with SPSS 12.0. Error bars indicate the average ODV numbers per cell-section (means ± standard deviations).

248.6 ± 19.6, and 316.5 ± 29.5 for WT, HaBacΔ*76*-$R_{1–816}$, HaBacΔ*76*-$R_{\Delta CR1–3}$, HaBacΔ*76*-$R_{\Delta CR1}$, HaBacΔ*76*-$R_{\Delta CR2}$, and HaBacΔ*76*-$R_{\Delta CR3}$, respectively (Fig. 7B). Further statistical analysis revealed no significant difference ($p > 0.05$) in the average ODV numbers in cells infected with WT or with HaBacΔ*76*-$R_{1–816}$ ($p = 0.48$), HaBacΔ*76*-$R_{\Delta CR1–3}$ ($p = 0.24$), HaBacΔ*76*-$R_{\Delta CR1}$ ($p = 0.25$), HaBacΔ*76*-$R_{\Delta CR2}$ ($p = 0.93$) or HaBacΔ*76*-$R_{\Delta CR3}$ ($p = 0.98$).

Together, these results suggested that the cysteine-rich region is important for OB morphogenesis and affects the morphology of OB along with the numbers of embedded ODVs. In addition, within the cysteine-rich region, CR1 appears to play a more critical role than CR2 and CR3.

3.8. The cysteine-rich region of HA76, particularly CR1, is essential for oral infection

Oral feeding assays were conducted with 1×10^8 OBs mL^{-1} on third instar *H. armigera* larvae. As shown in Table 1, the cysteine-rich region truncations HaBacΔ*76*-$R_{\Delta CR1–3}$ and HaBacΔ*76*-$R_{\Delta CR1}$ almost completely lost oral infectivity, leading to a mortality of < 5% with a concentration of 1×10^8 OB mL^{-1} during the feeding assay. Further bioassay (Table 2) showed that the LD_{50} of the repaired viruses HaBacΔ*76*-$R_{1–816}$ and HaBacΔ*76*-$R_{\Delta CR3}$ did not significantly differ from that of the WT, whereas the LD_{50} of HaBacΔ*76*-$R_{\Delta CR2}$ was approximately 1000-fold higher than that of the WT. Taken together, the results suggested that the N-terminal cysteine-rich region of HA76 is essential for oral infection, within which CR1 appears to be the most critical domain, with CR2 having a lesser degree of impact whereas CR3 did not impact oral infection.

Table 1
Feeding test of the recombinant viruses on *H. armigera* 3rd instar larvae.

Virus	Test 1	Test 2
	Dead/Total	Dead/Total
WT	48/48	48/48
HaBacΔ*76*-$R_{1–816}$	48/48	48/48
HaBacΔ*76*-$R_{\Delta 1–446}$	1/48	0/48
HaBacΔ*76*-$R_{\Delta CR1}$	2/48	1/48
HaBacΔ*76*-$R_{\Delta CR2}$	40/48	41/48
HaBacΔ*76*-$R_{\Delta CR3}$	47/48	48/48
Mock	0/48	0/48

3.9. Deletion of the cysteine-rich region does not affect HA76 incorporation into ODVs

As HA76 is a structural protein of ODV, we further investigated whether the truncation of the cysteine-rich region affected the incorporation of HA76 into ODV. Western blots were conducted with ODVs of WT HearNPV, HaBacΔ*76*-$R_{1–816}$, HaBacΔ*76*-$R_{\Delta CR1}$, HaBacΔ*76*-$R_{\Delta CR2}$, HaBacΔ*76*-$R_{\Delta CR3}$, and HaBacΔ*76*-$R_{\Delta CR1–3}$; the results showed that HA76 could be detected in all the ODVs (Fig. 8). The expected protein size of HA76, $HA76_{\Delta CR1}$, $HA76_{\Delta CR2}$, $HA76_{\Delta CR3}$, and $HA76_{\Delta CR1–3}$ should be 93, 81, 86, 82, and 62 kDa respectively, whereas the observed sizes were approximately 100, 90, 96, 90, and 70 kDa. The difference between the expected size and observed size was about 7–10 kDa and was consistent among all the recombinant viruses, suggesting that the protein modification of HA76 occurred at the either the N-terminal 1–135 or C-terminal 406–816 aa, which were retained in these viruses. An additional band of 70 or 65 kDa was found in the ODVs of HaBacΔ*76*-$R_{\Delta CR1}$ and HaBacΔ*76*-$R_{\Delta CR3}$, respectively, which may be due to protein cleavage or degradation.

4. Discussion

In the present study, we showed that *ha76* of HearNPV, a homologue of *vp91*, is a multifunctional gene. Many of our results are in agreement with previous findings on homologues for *vp91*. For example, our analysis showed that *ha76* is a late gene (Fig. 1), likewise, *vp91* was identified to be a late gene in AcMNPV, BmNPV and OpMNPV (Zhu et al., 2013; Lu et al., 1998; Russell and Rohrmann, 1997). The sub-cellular localization of HA76 (Fig. 2) was found to be in the ring-zone region at the late stage of infection, similar pattern was also found with VP91 homologues in AcMNPV and OpMNPV (Zhu et al., 2013; Javed et al., 2017; Russell and Rohrmann, 1997). Like *ac83* (Zhu et al., 2013; Huang et al., 2017; Javed et al., 2017) and *bm95* (Xiang et al., 2013), *ha76* is essential for nucleocapsid assembly and consequent BV production (Figs. 4 and 5). The region in *ha76* that is critical for nucleocapsid assembly (aa 406–816 or nt 1218–2448) is still larger than the NAE region identified in *ac83* (nt 1651–1850) (Huang et al., 2017); further experiment are needed to identify the NAE region in *ha76*. In AcMNPV, the N-terminal of VP91, especially the CR2 region was found to be critical for orally infectivity (Javed et al., 2017; Zhu et al., 2013) and similarly, we found the N-terminal and CR2 of HA76 to be important for oral infectivity (Table 2).

There are some minor dissimilarities between our results and previous studies. For example, the localization of HA76 in ODVs (Fig. 3A) is consistent with that of AcMNPV and OpMNPV, but with slight difference on the detailed localization within ODV. We found that HA76 is

Table 2
Bioassay results of the recombinant viruses on *H. armigera* 3rd instar larvae.

Virus	Test1		Test2	
	LD_{50}(OBs/mL)	Potency ratio (95% CI)	LD_{50}(OBs/mL)	Potency ratio (95% CI)
WT	1.06×10^4		1.6×10^4	
HaBacΔ*76*-$R_{1–816}$	0.9×10^4	1.192 (0.214–5.417)	1.5×10^4	1.066 (0.196–5.903)
HaBacΔ*76*-$R_{\triangle CR2}$	2.1×10^7	0 (1.81×10^{-6}–0.15)	2.06×10^7	0.01 (6.66×10^{-7}–0.031)
HaBacΔ*76*-$R_{\triangle CR3}$	1.4×10^4	0.721 (0.162–2.974)	2.1×10^4	0.749 (0.132–3.869)

OB: occlusion body; CI: confidence interval.

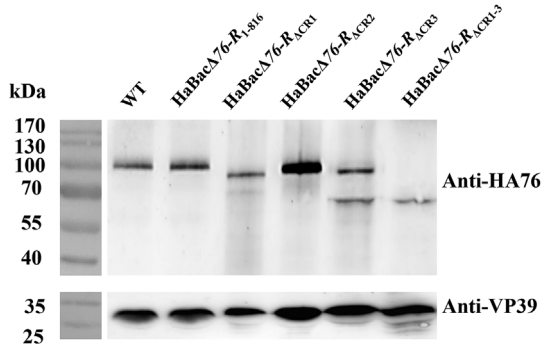

Fig. 8. Western blot analysis of HA76 in occlusion-derived viruses (ODVs) of the recombinant viruses. The purified ODVs from 1×10^9 occlusion bodies (OBs) of WT and HaBacΔ*76*-$R_{1–816}$, HaBacΔ*76*-$R_{\Delta CR1}$, HaBacΔ*76*-$R_{\Delta CR2}$, and HaBacΔ*76*-$R_{\Delta CR3}$, or from 5×10^9 OBs of HaBacΔ*76*-$R_{\Delta CR1–3}$ were used for each lane. Western blot analysis was performed using anti-HA76 as the primary antibody.

located in both the envelope and the nucleocapsid fractions of ODV (Fig. 3A), likewise, Javed et al. (2017) found that AC83 was detected mainly in the envelope of ODV but with a small amount in the nucleocapsid fraction. While in other studies, VP91 homologues were found solely in the envelope fraction of ODV (Zhu et al., 2013; Russell and Rohrmann, 1997; Hou et al., 2013). The localization of VP91 homologues in BVs is also controversial. We were unable to detect HA76 in BVs (Fig. 3B), even with 10 times more BVs (data not shown). Initially, Ac83 was not identified in BVs by Western blot (Zhu et al., 2013), but later it was found in AcMNPV BVs (Javed et al., 2017) like that of OpMNPV (Russell and Rohrmann, 1997). These inconsistences will likely to be explained as we get to know more about the molecular functions of VP91.

Most importantly, our results revealed a novel function of *ha76*, whereby it plays a critical role in OB morphogenesis by affecting the development of the polyhedral envelope (PE) (Fig. 6A and B) as well as in the embedding efficiency of the ODVs (Figs. 6C and 7).The OBs are composed of the protein matrix that occludes the ODVs and a surrounding membrane PE (Rohrmann, 2013). The major component of the protein matrix is polyhedrin, which forms trimers, which are arranged into dodecamers via disulfide bonds to form the crystal OB (Ji et al., 2010; Coulibaly et al., 2009). The PE is a smooth and electron-dense structure that surrounds and protects OBs, and is composed of carbohydrate and an integral phosphorylated protein PP34 or PE protein (PEP) (Minion et al., 1979; Whitt and Manning, 1988; Russell and Rohrmann, 1990). In baculovirus-infected cells, PEP is associated with the fibrillar structures formed by P10 and both proteins are required for proper assembly of the PE. Deletion of either *p10* or *pep* leads to the formation of OBs with a rough pitted surface and a fragmented or absent PE (Williams et al., 1989). The fragmented and pitted surface of OBs observed in the recombinant viruses of HaBacΔ*76*-$R_{\Delta CR1–3}$ and HaBacΔ*76*-$R_{\Delta CR1}$ (Fig. 6A and B) resembled those of the *pep* and/or *p10* deletion mutants (Williams et al., 1989). Therefore, apart from the previous reported *pep* and *p10*, *ha76* is the third baculovirus gene identified to date that is associated with the development of PE. Although the specific role of *ha76* in PE formation remains unclear, our findings indicated that CR1 of HA76 is critical for this function.

HaBacΔ*76*-$R_{\Delta CR1–3}$ and HaBacΔ*76*-$R_{\Delta CR1}$ produced significantly fewer embedded ODVs than the WT or HA76 repaired virus (Figs. 6C and 7), suggesting that HA76 is also involved in ODV occlusion. In a baculovirus-infected cell, nucleocapsids are first assembled by packing genomic DNA into the capsid at the virogenic stroma, followed by transport to the ring zone region where some capsids will egress to become BVs (Blissard and Theilmann, 2018), whereas others will be wrapped by viral-induced intranuclear membrane-derived microvesicles to form ODVs and finally be embedded into OBs (Slack and Arif, 2007). Consequently, the viral genes reported to be involved in ODV occlusion can be classified into the following classes: i) affecting nucleocapsid formation; ii) associated with the transport of nucleocapsids to the ring zone; iii) affecting the morphogenesis of microvesicles or ODV envelopment; iv) mutations of polyhedrin or affecting polyhedrin expression; and v) others, such as *p33*, which encodes a sulfhydryl oxidase involved in disulfide bond formation (Wu and Passarelli, 2010; Kuang et al., 2016, 2017). In HearNPV, a unique gene *ha83*, was also found to be involved in ODV embedding (Yu et al., 2015). The impact of the cysteine-rich region of HA76 on ODV embedding does not occur at the steps of nucleocapsid assembly or transportation to the ring zone, as evidenced by the normal production of BVs by all mutants (Fig. 4D). It is also unlikely to be at the stages of ODV envelopment, because the ODVs in the OBs of HaBacΔ*76*-$R_{\Delta CR1–3}$ and HaBacΔ*76*-$R_{\Delta CR1}$ were apparently encased with envelopes (Fig. 6). As HA76 is an ODV structural protein (Fig. 3), we thus speculated that the HA76 might instead be involved in the interaction of ODVs with polyhedrin for embedding.

In our study, CR1 domain appears to play a more critical role in OB morphology and ODV occlusion than CR2 or CR3 (Figs. 6 and 7A). Among the three ZF motifs previously identified in AcMNPV VP91 (Javed et al., 2017), only a C2H2-type ZF in CR1 is conserved in all VP91 proteins of baculoviruses (Fig. S1). C2H2-type ZF proteins form a very large family and have diverse functions including protein-protein interaction(Seetharam and Stuart, 2013). In the future, it will be interesting to reveal the role of the ZF in VP91 by constructing specific mutants and studying their impacts.

Notably, the OB morphology with ragged surfaces found in HaBacΔ*76*-$R_{\Delta CR2}$ and HaBacΔ*76*-$R_{\Delta CR3}$ (Fig. 6) resembled those of *p33* mutants in AcMNPV (Kuang et al., 2017). The latter also contain fewer ODVs in the OBs (Kuang et al., 2017). It was reported that PEP and a subpopulation of polyhedrin are thiol linked to PE (Whitt and Manning, 1988). The similar phenomena afforded by the cysteine-rich region mutants of HA76 to that of the mutants of sulfhydryl oxidase (P33) indicated that disulfide bond formation maybe involved in the role of HA76 on OB morphogenesis. The cysteine rich region of HA76 contains 18 cysteines, which are largely conserved among baculoviruses (Fig. 4A, Fig. S1). Although our results showed that CR1 is the most critical region for OB morphogenesis, considering the potential complexity of forming disulfide bonds among the cysteines, regions CR1–3 may function together. This is supported by the TEM/SEM results wherein the deletion of CR1–3 exerted a more serious effect on ODV

embedding than the deletion of CR1 alone (Figs. 6C and 7A). Future studies on the structure of VP91 will be helpful to understand the molecular mechanism of this multifunctional protein.

In accordance with the phenomena of pitted OBs and significantly fewer embedded ODVs, the oral infectivity of HaBacΔ*76*-$R_{\Delta CR1-3}$ and HaBacΔ*76*-$R_{\Delta CR1}$ were significantly lower than that of the WT (Table 1) and their LD_{50} was too high to be measured, suggesting that the influence on OB morphogenesis severely impacted oral infectivity. However, HaBacΔ*76*-$R_{\Delta CR2}$, which apparently contained normal numbers of encased ODVs (Figs. 6C and 7A), also showed a significant reduction in oral infectivity, with an LD_{50} approximately 1000-fold higher than that of the WT (Table 2). This result is consistent with previous results of AcMNPV VP91, that CR2 plays a critical role for oral infectivity (Zhu et al., 2013; Javed et al., 2017). The results suggested that other factors exist that contribute to the role of VP91 in oral infectivity. In fact, AcMNPV VP91 (PIF8) has been shown to serve as a component of the PIF complex (Wang et al., 2017, 2019; Peng et al., 2012; Boogaard et al., 2018; Javed et al., 2017). Therefore, the role of HA76 in oral infectivity is likely only partly due to its impact on OB morphogenesis.

Acknowledgements

This research was supported by the grants from the National Key R& D Program of China (2017YFD0200400), the Key Research Project of Frontier Science (QYZDJ-SSW-SMC021) and Strategic Priority Research Program (grant No. XDB11030400) from the Chinese Academy of Sciences, and the grants (No. 31570153, 31621061 and 31130058) from the National Natural Science Foundation of China. The authors would like to thank Bi-Chao Xu of the Core Facility and Technical Support of Wuhan Institute of Virology for technical assistance.

Appendix A. Supplementary data

Supplementary data to this article can be found online at https://doi.org/10.1016/j.virol.2019.06.016.

References

Blissard, G.W., Theilmann, D.A., 2018. Baculovirus entry and egress from insect cells. Annu. Rev. Virol. 5, 113–139.
Boogaard, B., van Oers, M.M., van Lent, J.W.M., 2018. An advanced view on baculovirus per os infectivity factors. Insects 9.
Braunagel, S.C., Summers, M.D., 1994. Autographa californica nuclear polyhedrosis virus, PDV, and ECV viral envelopes and nucleocapsids: structural proteins, antigens, lipid and fatty acid profiles. Virology 202, 315–328.
Burand, J.P., Kim, W., Afonso, C.L., Tulman, E.R., Kutish, G.F., Lu, Z.Q., Rock, D.L., 2012. Analysis of the genome of the sexually transmitted Insect virus Helicoverpa zea nudivirus 2. Viruses-Basel 4, 28–61.
Chen, X., WF, I.J., Tarchini, R., Sun, X., Sandbrink, H., Wang, H., Peters, S., Zuidema, D., Lankhorst, R.K., Vlak, J.M., Hu, Z., 2001. The sequence of the Helicoverpa armigera single nucleocapsid nucleopolyhedrovirus genome. J. Gen. Virol. 82, 241–257.
Chen, Y.R., Zhong, S., Fei, Z., Hashimoto, Y., Xiang, J.Z., Zhang, S., Blissard, G.W., 2013. The transcriptome of the baculovirus Autographa californica multiple nucleopolyhedrovirus in Trichoplusia ni cells. J. Virol. 87, 6391–6405.
Coulibaly, F., Chiu, E., Gutmann, S., Rajendran, C., Haebel, P.W., Ikeda, K., Mori, H., Ward, V.K., Schulze-Briese, C., Metcalf, P., 2009. The atomic structure of baculovirus polyhedra reveals the independent emergence of infectious crystals in DNA and RNA viruses. Proc. Natl. Acad. Sci. U. S. A 106, 22205–22210.
Deng, F., Wang, R., Fang, M., Jiang, Y., Xu, X., Wang, H., Chen, X., Arif, B.M., Guo, L., Wang, H., Hu, Z., 2007. Proteomics analysis of Helicoverpa armigera single nucleocapsid nucleopolyhedrovirus identified two new occlusion-derived virus-associated proteins, HA44 and HA100. J. Virol. 81, 9377–9385.
Harrison, R.L., Herniou, E.A., Jehle, J.A., Theilmann, D.A., Burand, J.P., Becnel, J.J., Krell, P.J., van Oers, M.M., Mowery, J.D., Bauchan, G.R., Ictv Report, C., 2018. ICTV virus taxonomy profile: Baculoviridae. J. Gen. Virol. 99, 1185–1186.
Hou, D.H., Zhang, L.K., Deng, F., Fang, W., Wang, R.R., Liu, X.J., Guo, L., Rayner, S., Chen, X.W., Wang, H.L., Hu, Z.H., 2013. Comparative proteomics reveal fundamental structural and functional differences between the two progeny phenotypes of a baculovirus. J. Virol. 87, 829–839.
Huang, H., Wang, M., Deng, F., Wang, H., Hu, Z., 2012. ORF85 of HearNPV encodes the per os infectivity factor 4 (PIF4) and is essential for the formation of the PIF complex. Virology 427, 217–223.
Huang, Z., Pan, M., Zhu, S., Zhang, H., Wu, W., Yuan, M., Yang, K., 2017. The Autographa californica multiple nucleopolyhedrovirus ac83 gene contains a cis-acting element that is essential for nucleocapsid assembly. J. Virol. 91.
Hughes, P.R., Vanbeek, N.A.M., Wood, H.A., 1986. A modified droplet feeding method for rapid assay of bacillus-thuringiensis and baculoviruses in noctuid larvae. J. Invertebr. Pathol. 48, 187–192.
Javed, M.A., Biswas, S., Willis, L.G., Harris, S., Pritchard, C., van Oers, M.M., Donly, B.C., Erlandson, M.A., Hegedus, D.D., Theilmann, D.A., 2017. Autographa californica multiple nucleopolyhedrovirus AC83 is a per Os infectivity factor (PIF) protein required for occlusion-derived virus (ODV) and budded virus nucleocapsid assembly as well as assembly of the PIF complex in ODV envelopes. J. Virol. 91.
Ji, X.Y., Sutton, G., Evans, G., Axford, D., Owen, R., Stuart, D.I., 2010. How baculovirus polyhedra fit square pegs into round holes to robustly package viruses. EMBO J. 29, 505–514.
Kuang, W., Zhang, H., Hou, D., Wang, M., Deng, F., Wang, H., Hu, Z., 2016. P33 of Helicoverpa armigera single nucleocapsid nucleopolyhedrovirus is a functional homolog of AcP33. Virol. Sin. 31, 346–349.
Kuang, W., Zhang, H., Wang, M., Zhou, N.Y., Deng, F., Wang, H., Gong, P., Hu, Z., 2017. Three conserved regions in baculovirus sulfhydryl oxidase, P33, are critical for enzymatic activity and function. J. Virol.
Liu, J., Zhu, L., Zhang, S., Deng, Z., Huang, Z., Yuan, M., Wu, W., Yang, K., 2016. The Autographa californica multiple nucleopolyhedrovirus ac110 gene encodes a new per os infectivity factor. Virus Res. 221, 30–37.
Long, G., Westenberg, M., Wang, H., Vlak, J.M., Hu, Z., 2006. Function, oligomerization and N-linked glycosylation of the Helicoverpa armigera single nucleopolyhedrovirus envelope fusion protein. J. Gen. Virol. 87, 839–846.
Lu, M., Swevers, L., Iatrou, K., 1998. The p95 gene of Bombyx mori nuclear polyhedrosis virus: temporal expression and functional properties. J. Virol. 72, 4789–4797.
Mcintosh, A.H., Ignoffo, C.M., 1983. Characterization of 5 cell-lines established from species of Heliothis. Appl. Entomol. Zool. 18, 262–269.
Minion, F.C., Coons, L.B., Broome, J.R., 1979. Characterization of the polyhedral envelope of the nuclear polyhedrosis-virus of Heliothis-Virescens. J. Invertebr. Pathol. 34, 303–307.
Peng, K., van Lent, J.W., Boeren, S., Fang, M., Theilmann, D.A., Erlandson, M.A., Vlak, J.M., van Oers, M.M., 2012. Characterization of novel components of the baculovirus per os infectivity factor complex. J. Virol. 86, 4981–4988.
Peng, K., van Lent, J.W., Vlak, J.M., Hu, Z., van Oers, M.M., 2011. In situ cleavage of baculovirus occlusion-derived virus receptor binding protein P74 in the peroral infectivity complex. J. Virol. 85, 10710–10718.
Robertson, J.L., Jones, M.M., Olguin, E., Alberts, B., 2017. Bioassays with Arthropods. CRC press.
Rohrmann, G.F., 2013. Baculovirus Molecular Biology, Bethesda (MD). in: rd (Ed.).
Russell, R.L., Rohrmann, G.F., 1990. A baculovirus polyhedron envelope protein: immunogold localization in infected cells and mature polyhedra. Virology 174, 177–184.
Russell, R.L., Rohrmann, G.F., 1997. Characterization of P91, a protein associated with virions of an Orgyia pseudotsugata baculovirus. Virology 233, 210–223.
Seetharam, A., Stuart, G.W., 2013. A study on the distribution of 37 well conserved families of C2H2 zinc finger genes in eukaryotes. BMC Genomics 14, 420.
Slack, J., Arif, B.M., 2007. The baculoviruses occlusion-derived virus: virion structure and function. Adv. Virus Res. 69, 99–165.
Song, J., Wang, R., Deng, F., Wang, H., Hu, Z., 2008. Functional studies of per os infectivity factors of Helicoverpa armigera single nucleocapsid nucleopolyhedrovirus. J. Gen. Virol. 89, 2331–2338.
Sun, X., Zhang, G., Zhang, Z., Hu, Z., Vlak, J., Arif, B., 1997. In vivo cloning of Helicoverpa armigera single nucleocapsid nuclear polyhedrosis virus genotypes. Virol. Sin. 13, 83–88.
Sun, X.L., 2015. History and current status of development and use of viral insecticides in China. Viruses-Basel 7, 306–319.
Wang, H.Z., Deng, F., Pijlman, G.P., Chen, X.W., Sun, X.L., Vlak, J.M., Hu, Z.H., 2003. Cloning of biologically active genomes from a Helicoverpa armigera single-nucleocapsid nucleopolyhedrovirus isolate by using a bacterial artificial chromosome. Virus Res. 97, 57–63.
Wang, X., Liu, X., Makalliwa, G.A., Li, J., Wang, H., Hu, Z., Wang, M., 2017. Per os infectivity factors: a complicated and evolutionarily conserved entry machinery of baculovirus. Sci. China Life Sci. 60, 806–815.
Wang, X., Shang, Y., Chen, C., Liu, S., Chang, M., Zhang, N., Hu, H., Zhang, F., Zhang, T., Wang, Z., Liu, X., Lin, Z., Deng, F., Wang, H., Zou, Z., Vlak, J.M., Wang, M., Hu, Z., 2019. Baculovirus per os infectivity factor complex:components and assembly. J. Virol.
Wang, Y.J., Kleespies, R.G., Huger, A.M., Jehle, J.A., 2007. The genome of Gryllus bimaculatus nudivirus indicates an ancient diversification of baculovirus-related nonoccluded nudiviruses of insects. J. Virol. 81, 5395–5406.
Whitt, M.A., Manning, J.S., 1988. A phosphorylated 34-kDa protein and a subpopulation of polyhedrin are thiol linked to the carbohydrate layer surrounding a baculovirus occlusion body. Virology 163, 33–42.
Williams, G.V., Rohel, D.Z., Kuzio, J., Faulkner, P., 1989. A cytopathological investigation of Autographa californica nuclear polyhedrosis virus p10 gene function using insertion/deletion mutants. J. Gen. Virol. 70 (Pt 1), 187–202.
Wu, W., Passarelli, A.L., 2010. Autographa californica multiple nucleopolyhedrovirus Ac92 (ORF92, P33) is required for budded virus production and multiply enveloped occlusion-derived virus formation. J. Virol. 84, 12351–12361.
Xiang, X., Shen, Y., Yang, R., Chen, L., Hu, X., Wu, X., 2013. Bombyx mori nucleopolyhedrovirus BmP95 plays an essential role in budded virus production and nucleocapsid assembly. J. Gen. Virol. 94, 1669–1679.
Yang, Y.T., Lee, D.Y., Wang, Y.J., Hu, J.M., Li, W.H., Leu, J.H., Chang, G.D., Ke, H.M., Kang, S.T., Lin, S.S., Kou, G.H., Lo, C.F., 2014. The genome and occlusion bodies of

marine Penaeus monodon nudivirus (PmNV, also known as MBV and PemoNPV) suggest that it should be assigned to a new nudivirus genus that is distinct from the terrestrial nudiviruses. BMC Genomics 15.
Yu, H., Xu, J., Liu, Q., Liu, T.X., Wang, D., 2015. Ha83, a chitin binding domain encoding gene, is important to Helicoverpa armigera nucleopolyhedrovirus budded virus production and occlusion body assembling. Sci. Rep. 5, 11088.
Zhu, S., Wang, W., Wang, Y., Yuan, M., Yang, K., 2013. The baculovirus core gene ac83 is required for nucleocapsid assembly and per os infectivity of Autographa californica nucleopolyhedrovirus. J. Virol. 87, 10573–10586.